

Role of salt concentration on conductivity optimization and structural phase separation in a solid polymer electrolyte based on PMMA-LiClO₄

Namrata Shukla · Awalendra K. Thakur

Received: 4 June 2008 / Accepted: 11 September 2008 / Published online: 7 October 2008
© Springer-Verlag 2008

Abstract Although a large number of ionic conductors based on poly(methyl-methacrylate) (PMMA) are reported in literature, an optimization of salt concentration with respect to conductivity and stability properties remains by and large neglected. We report, perhaps for the first time, such an optimization of salt (LiClO₄) concentration on structural, morphological, electrical, and ion–polymer interaction in PMMA-based solid polymer films. The active coordination site for the cation (Li⁺), out of the two possible electron donating functional groups (i.e. C=O and O–CH₃) in PMMA, has been ascertained on the basis of evidences recorded in Fourier transform infrared spectrum. The results suggested C=O as the only possible site in PMMA matrix for coordination with Li⁺ cation. The X-ray diffraction results have clearly indicated an optimum limit of salt dissolution in PMMA matrix corresponding to O/Li = 4 (i.e., ~21wt.%) above which “phase-separation” occurs distinctly. The effect of salt concentration on amorphous → crystalline phase changes in PMMA and its correlation to morphology have been clearly observed in terms of their impact on electrical properties. An optimum electrical conductivity of $\sim 7.2 \times 10^{-5} \text{ S cm}^{-1}$ has been recorded at 100°C (~PMMA glass transition). The temperature dependence of conductivity follows typical Vogel–Tamman–Fulcher behavior.

Keywords Polymer Electrolytes · FTIR · XRD · DC conductivity

Introduction

Ionically conducting solid polymer electrolyte (SPE) membranes based on salts dissolved in an appropriate polymer matrix has received considerable attention due to a number of desirable properties such as design flexibility, leak free behavior, miniaturization feasibility, improved safety, and ease of device fabrication, etc. Furthermore, an ionically conducting polymer membrane for electrochemical device applications should have a proper balance between its conductivity and mechanical strength (i.e., high ionic conductivity and good mechanical strength) under the conditions desirable for a specific application. This requires a meticulous optimization of various desirable properties of the material system, which in turn is predominantly controlled by the stoichiometric ratio of the polymer–salt combination in a SPE. SPEs, having optimized conductivity and stability properties under ambient and sub-ambient conditions, may be expected to have potential for applications in solid-state ionic devices such as the high energy density batteries, supercapacitors, etc.

Literature reveals that electrical transport properties in a polymer occur through the amorphous phase rather than crystalline [1]. In view of this notion concluded from nuclear magnetic resonance spectroscopy data, it appears more appropriate to select a polymer host that is predominantly amorphous such as PMMA having ~96% amorphous content at 25°C [2]. In addition, PMMA is a lightweight and transparent polymer having lesser reactivity toward lithium-metal-based anode, thereby providing scope for the improvement of electrode–electrolyte interfacial stability. These expected advantages provided substantial impetus to modify PMMA, which is predominantly insulating with only electronic transport, into an ionically conducting system. Subsequently, a number of ionically

N. Shukla · A. K. Thakur (✉)
Department of Physics and Meteorology,
Indian Institute of Technology,
Kharagpur 721302, India
e-mail: akt@phy.iitkgp.ernet.in

conducting SPE and gel polymer electrolyte based on PMMA with different combinations of salts and solvents, such as PMMA-LiClO₄ [3–5], PMMA-LiCF₃SO₃ [4–7], PMMA-NH₄CF₃SO₃ [8], PMMA-LiBF₄ [9], PMMA-LiAsF₆ [4], PMMA-Li₂SO₄ [10], with solvents such as acetonitrile, ethylene carbonate, and propylene carbonate, etc. have been reported in the literature.

However, two important aspects; (1) the optimized salt concentration having maximum conductivity in a PMMA-salt based complexes (PS) and (2) the identification of cation coordination site in the PMMA matrix that comprises of two probable solvating heteroatom/polar functional groups (i.e., C=O, O–CH₃) with electron donating ability, have not yet been specified in literature. Since salt concentration plays a crucial role in controlling conductivity level and determining the nature of interaction of the ions with the polymer matrix [11], no work on ionically conducting SPEs may be considered complete until an optimized salt concentration is known for a particular polymer host matrix. Additionally, if more than one site for cation coordination is present in the polymer matrix, then it becomes essential to know the actual site where ionic species are interacting with the polymer host in order to understand the state-of-the art system property.

In view of the facts mentioned above, we have taken up a systematic study on optimization of salt concentration to obtain an ultimate limit of salt dissolution in the PMMA matrix that leads to an optimized conductivity in the complexed (PMMA-LiClO₄) combination. PMMA-LiClO₄ complexation (PS) has been carried out over a wide range of salt concentration (variation of 2–35wt.% with respect to polymer) and expressed in terms of O/Li⁺ ratio varying over a wide range (i.e., O/Li⁺ ~25–2). The formula for calculation of O/Li⁺ is given below:

$$\frac{O}{Li^+} = \frac{\text{No. of monomer unit in 1 gm of PMMA}}{\text{No. of LiClO}_4 \text{ molecules in 1 gm of salt}} \times \frac{\text{wt. of PMMA taken}}{\text{wt. of salt taken}} \quad (1)$$

We have investigated the effect of salt concentration on structural phase formation, microstructural changes, ion-polymer interaction, and ion-transport properties.

Experimental

Materials preparation

Polymer electrolyte films were prepared by means of standard solution cast technique. PMMA (Aldrich M.W. $\sim 2 \times 10^5$) was used as the polymer host matrix and LiClO₄ (Acros Organics, USA) as the salt for complexation. The polymer host (PMMA) was vacuum-dried, and the salt (LiClO₄) was

dried at a temperature $\sim 150^\circ\text{C}$ for 24h to remove surface absorbed moisture content prior to sample preparation. An appropriate stoichiometric ratio of PMMA was dissolved in acetonitrile (Merck), and the solution was stirred for 12h. Subsequently, calculated amount of LiClO₄ was added and stirred for 12h to facilitate homogeneous mixing and complexation. The resulting final polymer-salt complex solution for each salt concentration was cast into films in polypropylene dishes, and the solvent was allowed to evaporate slowly at room temperature (27°C). The solvent-evaporated free-standing polymer-salt complex (PS) films were finally vacuum-dried at 40°C to remove residual solvent, if any, and stored in an inert medium for further analysis.

Materials characterization

The X-ray diffraction (XRD) pattern were recorded at room temperature using a Philips X'Pert Pro PANalytical diffractometer (model PW 3040/60) with CuK α radiation ($\lambda = 1.5418\text{\AA}$) over a range of diffraction angles: $10^\circ \leq 2\theta \leq 60^\circ$ at a scanning rate $\sim 4^\circ \text{ min}^{-1}$. The surface morphology and its variation with salt concentration were studied by Optical Microscopy (Nikon, Japan). Fourier transform infrared (FTIR) spectrum were collected in the mid-frequency range ($4,000\text{cm}^{-1}$ to 400cm^{-1}) at an average scan rate of 32 with spectral resolution of 4cm^{-1} using Thermo Nicolet Spectrophotometer (model Nexus-870). Complex impedance spectrum (CIS) measurements on the sample films were performed for samples of various salt concentration over a range of temperature (room temperature– 150°C) using a computer interfaced impedance analyzer (HIOKI LCR Hi-Tester, Model: 3522-50, Japan) in the frequency range of 0.1Hz to 100KHz. The sample cells having a configuration; SS|PS|SS were placed in a self-designed sample holder for electrical measurements (SS stands for stain less steel blocking electrodes and PS is for polymer-salt complex). An AC input signal of $\sim 200\text{mV}$ (peak to peak) was applied across the cell prior to start of the measurements.

Results and discussion

XRD analysis

The XRD pattern of PMMA-LiClO₄ complexes for various salt concentrations (estimated and implemented in terms of O/Li ratio or w/w w.r.t. polymer) is shown in Figs. 1 and 2. The XRD pattern of pure PMMA has its characteristic peaks observed at angles (2θ) $\sim 13.47^\circ$, 23° , 30.5° , and 42° out of which the peak at the 13.47° is moderately sharp (diffused), and the remaining peaks are markedly weak in intensity and appear in the broad halo region towards higher

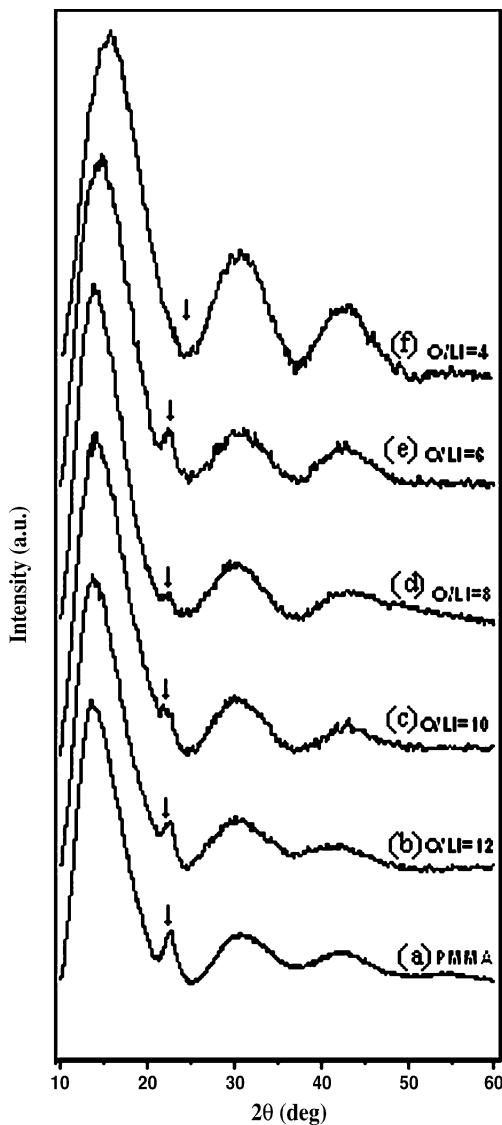


Fig. 1 XRD pattern of **a** PMMA and PMMA-LiClO₄ with **b** O/Li=12, **c** O/Li=10, **d** O/Li=8, **e** O/Li=6, and **f** O/Li=4

angle side. Such a pattern suggests a predominantly amorphous phase of the host polymer (PMMA). The addition of salt (LiClO₄) into PMMA matrix results in substantial modification of XRD pattern noticed in terms of (1) a systematic shift in PMMA main peak position (13.47°) toward higher angle side up to a salt concentration of 21wt.% (~O/Li = 4), (2) a systematic and consistent broadening of PMMA peak with increase in salt concentration, and (3) a gradual decrease in the intensity of PMMA peak (23°) with an increase in salt concentration that eventually vanishes at O/Li ~4 (21wt.%) salt concentration. A shift of XRD peak towards the higher angle side results due to the increase in d-spacing of the polymer matrix, suggesting evidence of the interaction of salt with PMMA and arising out of a possible complexation of cation (Li⁺ ion) with electron-rich site in the host polymer matrix.

The polymer–salt interaction (complexation) is also suggested by a gradual decrease in intensity of 23° peak on increasing the salt concentration that disappears for the sample film with O/Li ~4 but reappears for O/Li ~2 (shown in the Fig. 1). This may be a clear evidence of the optimum concentration limit of salt dissolution (i.e., O/Li ~4 ≡ 21wt.%) into the PMMA matrix. Beyond this concentration limit, an unambiguous testimony of polymer–salt “phase separation” has been observed, indicated by the presence of both the PMMA and salt (LiClO₄) peaks in the XRD pattern for PMMA-LiClO₄ (O/Li ~2) as shown in the Fig. 2. The XRD pattern of pure LiClO₄ has also been given in the Fig. 2 for comparison. The diffractogram of polymer–salt complex for O/Li ~2 shows sharp peaks in clear contrast to the XRD pattern of polymer–salt complex for all other salt concentra-

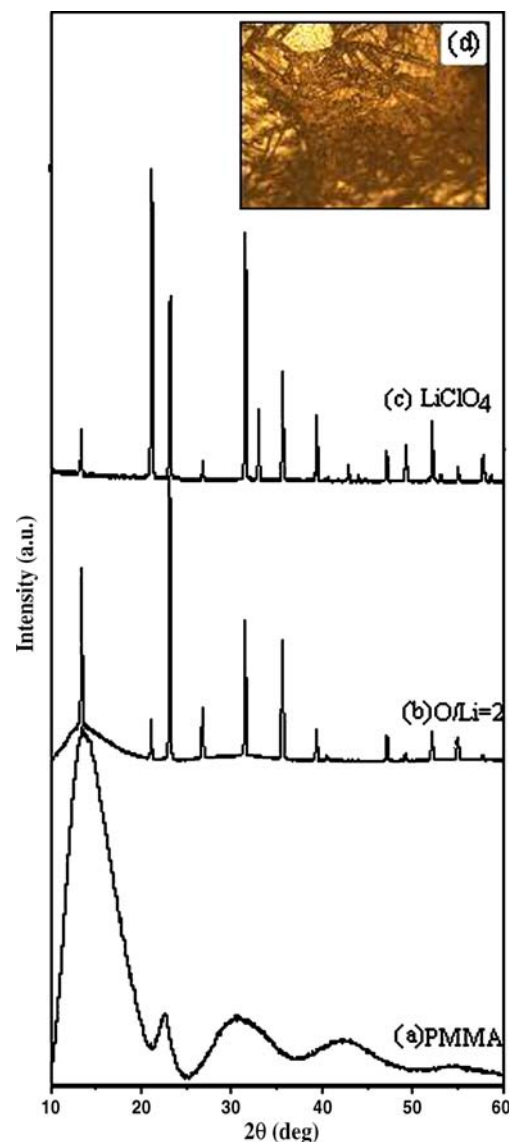


Fig. 2 XRD pattern of **a** PMMA, **b** PMMA-LiClO₄ (O/Li=2), **c** pure LiClO₄, **d** optical micrograph of O/Li=2

Table 1 X ray-diffraction and DC conductivity of PMMA–LiClO₄ (O/Li ~0–12) films

Salt ratio (O/Li)	PMMA main peak XRD data			Conductivity	
	d Spacing (Å)	Interchain spacing (Å)	% of amorphousness	T=30 °C	T=100 °C
0	6.57	8.22	85	1.0 × 10 ^{-16a}	1 × 10 ^{-13a}
12	6.47	8.1	85	1.27 × 10 ⁻¹⁰	3.89 × 10 ⁻⁷
10	6.45	8.1	82	9.95 × 10 ⁻¹¹	3.96 × 10 ⁻⁹
8	6.41	8.01	83	3.47 × 10 ⁻⁹	3.77 × 10 ⁻⁶
6	5.82	7.27	82	3.77 × 10 ⁻¹⁰	2.5 × 10 ⁻⁶
4	5.46	6.83	81	6.73 × 10 ⁻⁹	7.2 × 10 ⁻⁵
2	6.65	8.33	71	6.07 × 10 ⁻⁹	9.19 × 10 ⁻⁴

^a Pure PMMA conductivity as reported in literature [18]

tion in the range (O/Li ~18 to O/Li~4). A comparison suggests that the polymer salt complexes with O/Li = 2 and O/Li = 4 in the present studies represent basically two distinct types of polymer electrolytes. The former comprises of a mixed-phase solid polymer electrolyte consisting of polymer–salt complex (PS) and undissolved salt (LiClO₄). Both the PS and uncomplexed salt exist as the separate phase in the PS (PMMA–LiClO₄) matrix. An evidence of phase separation in the case of PMMA–LiClO₄ with O/Li = 2 has also been clearly observed in optical micrograph (inset of Fig. 2). On the other hand, PMMA–LiClO₄ with O/Li = 4 represents a solid polymer electrolyte composition where dissolution of the salt (LiClO₄) in the polymer host matrix has occurred up to a permissible saturation limit. Beyond this, an evidenced phase separation takes place. Such structural changes in the sample films with O/Li = 2 and

O/Li = 4 may be expected to reflect its impact in terms of their distinct electrical behavior.

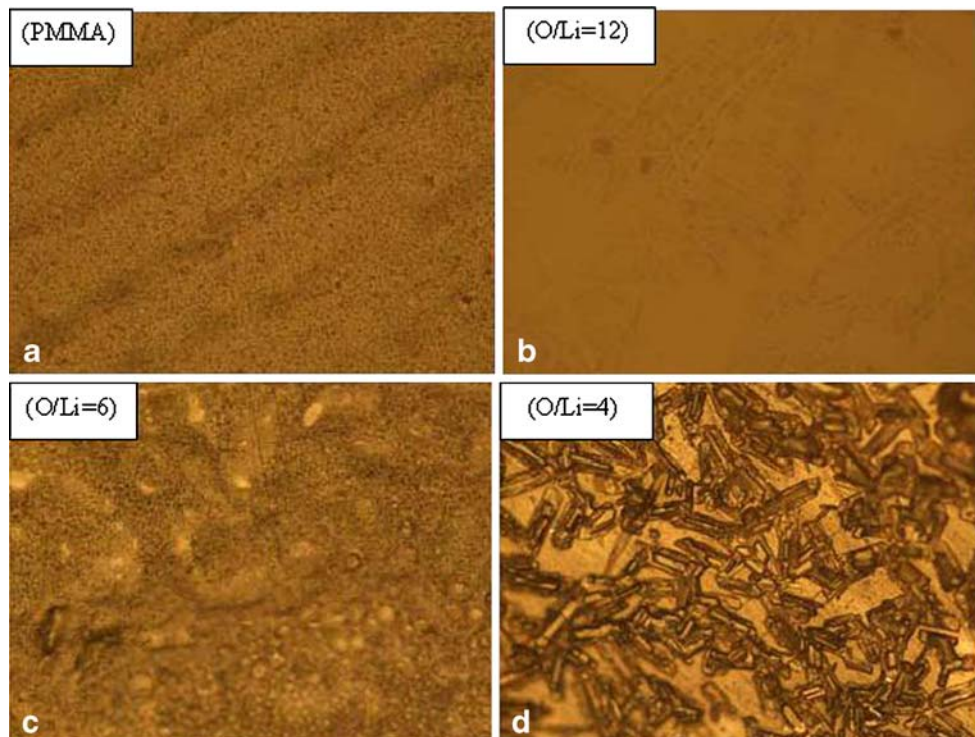
The effect of salt concentration on intrinsic structural parameters of the host polymer, i.e., d-spacing, and interchain separation (*R*) has been estimated from the sample XRD data in accordance with the following set of equations valid for predominantly non-crystalline samples and expressed as:

$$d = \lambda / 2 \sin \theta \quad (2)$$

$$R = 5/8(\lambda / \sin \theta) \quad (3)$$

where λ = X-ray wavelength ~1.5418Å. The calculated values of these parameters for the sample films with different salt concentration are given in Table 1. A

Fig. 3 Optical images for **a** pure PMMA and PMMA–LiClO₄, **b** O/Li=12, **c** O/Li=6, **d** O/Li=4



comparison shows systematic decrease in the interchain separation with increasing salt addition up to $O/Li \sim 4$ where it has the minimum cutoff value of $R \sim 6.83\text{\AA}$ beyond which it again retraces its value to a level ($R \sim 8.33\text{\AA}$) for $O/Li \sim 2$, which is higher than that of the pure PMMA ($R \sim 8.22\text{\AA}$). Almost a similar pattern is observed in the case of changes in other parameters such as the d-spacing and the degree of amorphosity, suggesting a sharp increase in the crystalline fraction for the sample with $O/Li \sim 2$ on comparison with rest of the samples. Furthermore, a change in the salt concentration has been observed to produce substantial changes in the flexibility and optical transparency of the films with a clear indication that the polymer–salt complex undergoes a drastic modification in its structural phase formation and microstructure at $O/Li \sim 4$ with a crossover in its phase characteristics, physical strength, and optical properties. It thus appears that there is an optimum limit of salt dissolution in PMMA beyond which even a small change in the concentration results in drastic modification of polymer phase characteristics, i.e., phase separation above the threshold limit indicated by the optical micrograph for $O/Li \sim 2$ shown in the inset of the Fig. 2. A better comparison of the role of salt concentration on the evolution of microstructural changes have been observed in optical microscopy and are described below.

Sample morphology

The optical micrographs of pure PMMA having typical features of smooth striations without any resolved surface topography are suggestive of its characteristic amorphous microstructure. The addition of even a very small quantity of salt ($O/Li \sim 12 \equiv 8\text{wt.}\%$) in the PMMA matrix brings substantial modification in the microstructural pattern when compared with that of pure PMMA shown in Fig. 3. Furthermore, an increase in the salt concentration has profound effect in changing the microstructure of PMMA from predominantly amorphous to an appreciably crystalline one. Such changes are in fact visible with change in salt concentration from 8wt.% ($\sim O/Li = 12$) up to the saturation limit of salt dissolution in PMMA matrix at salt concentration 21wt.% ($O/Li \sim 4$). Micrographs have also shown an evidence of phase separation observed in terms of PMMA- LiClO_4 complex and LiClO_4 salt appearing as two distinct phase for $O/Li \sim 2$ (i.e., 35wt.%). This change in microstructure revealed in optical microscopy agrees well with the observations of change in crystallinity and phase separation effect with salt concentration recorded in XRD analysis.

FTIR analysis

Figure 4 shows the FTIR spectrum of LiClO_4 and PMMA- LiClO_4 complexes for $O/Li = 12$ to 2 representing a broad

range of salt concentration varying from 0 to 35% w.r.t. PMMA (w/w). The spectral pattern shows noticeable changes in the vibrational modes of PMMA observed in terms of shifting band position, band width, and intensity with change in salt concentration. The FTIR bands corresponding to the molecular vibration of the various groups in the polymer–salt complex has been identified, and their assignment for various salt concentrations in the films is given in Table 2 for comparison and further analysis. It appears that the changes occurring in the spectrum observed in the wave number region $\sim 1,727$ – $1,732$, 843 , and 624cm^{-1} attributed respectively to $\nu(\text{C}=\text{O})_s$ [12], $\gamma(\text{CH}_2)_a + \nu(\text{C}-\text{O}-\text{C})_s$ and $\delta(\text{ClO}_4^-)$ are quite systematic and of general interest in the present studies. In the LiClO_4 spectrum, the bands present at (455 , 625 , 939 , and $1,099\text{cm}^{-1}$) are assigned to $\delta(\text{ClO}_4^-)_s$, $\delta(\text{ClO}_4^-)_a$ [14],

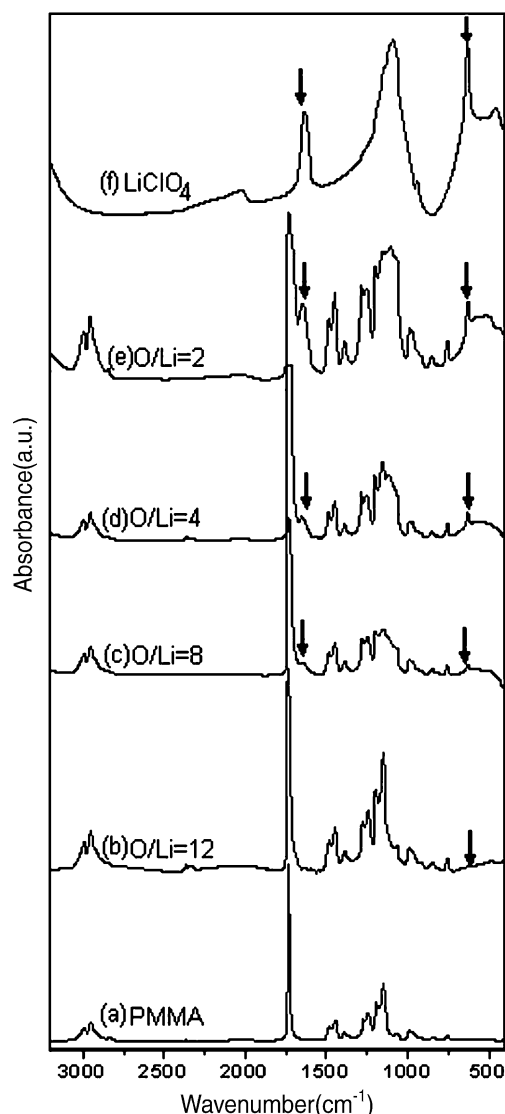


Fig. 4 FTIR plot for **a** PMMA and PMMA- LiClO_4 with **b** $O/Li=12$, **c** $O/Li=8$, **d** $O/Li=4$, **e** $O/Li=2$, **f** pure LiClO_4

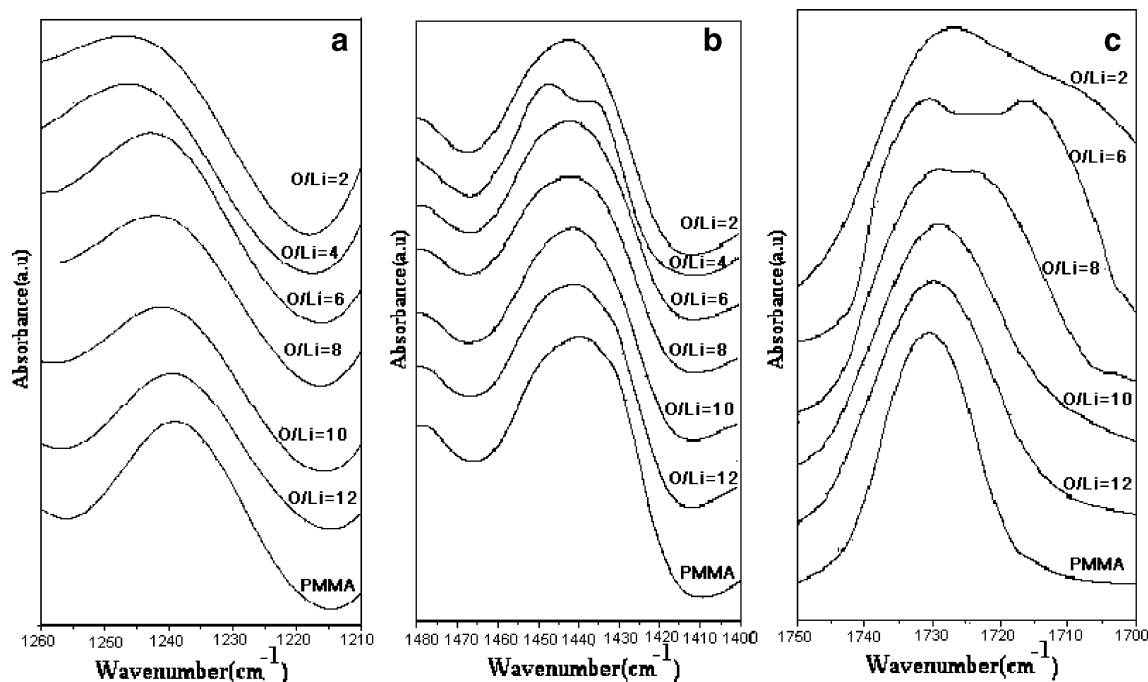
Table 2 FTIR band positions of PMMA–LiClO₄ (O/Li ~0–12) films and their assignment

FTIR band positions of PMMA- <i>x</i> LiClO ₄ (<i>x</i> =O/Li ratio w.r.t PMMA (w/w))							Band assignment	Ref.
PMMA	O/Li=12	O/Li=10	O/Li=8	O/Li=6	O/Li=4	O/Li=2		
–	625	626	626	625	626	626	$\delta(\text{ClO}_4^-)_a$	
760	752	753	752	753	751	752	$\gamma(\text{CH}_2)$	[13]
844	844	846	846	846	846	849	$\gamma(\text{CH}_2)_a + \nu(\text{C-O-C})_s$	
989	987	987	987	986	986	985	$\gamma(\text{CH}_2\text{-CH}) + \nu_s(\text{C-C})$	
–	–	–	–	–	–	1,099	$\nu(\text{Cl-O})$	[14]
1,150	1,150	1,151	1,149	1,151	1,153	1,153–	CH ₂ bending	[12]
1,192	1,192	1,193	1,196	1,194	1,197	1,196	$\nu(\text{C-H})_s, \text{C-O-C}$ bending	[12, 13]
1,242	1,242	1,242	1,242	1,242	1,242	1,242	$\nu(\text{OCH}_3)_s$ C–C–O stretch	[12]
1,271	1,273	1,273	1,279	1,277	1,280	1,280	$\nu(\text{C-O})_a$ in –COO–group	[13]
1,387	1,387	1,387	1,387	1,387	1,387	1,387	$\nu(\text{CH}_2)$ C–CH ₃ bending	[12]
1,444	1,444	1,444	1,444	1,445	1,444	1,444	C–O–C and $\nu(\text{O-CH}_3)_a$	
1,492	1,489	1,489	1,487	1,484	1,485	1,483	$\nu(\text{CH}_2)_a$	[12]
1,732	1,730	1,730	1,730	1,729	1,728	1,727	$\nu(\text{C=O})$	[12]
2,845	2,845	2,845	2,845	2,845	2,845	2,845	$\nu(\text{CH}_2)$	
2,951	2,951	2,951	2,952	2,952	2,954	2,954	$\nu(\text{C-H})_s$ of C–CH ₃	[12]
2,999	2,996	2,996	2,997	2,997	2,999	2,999	$\nu(\text{C-H})_a$ of O–CH ₃	[12]

$\nu(\text{ClO}_4^-)_s$ and $\nu(\text{ClO}_4^-)_a$ band. It appears that the changes occurring in the spectrum observed in the wave number region ~1,727–1,732, 843, and 624 cm⁻¹ attributed, respectively, to $\nu_s(\text{C=O})$ [12], $\gamma(\text{CH}_2)_a + \nu(\text{C-O-C})_s$ and $\nu_4(\text{ClO}_4^-)$ are quite systematic and of general interest in the present studies. A description of the changes so observed and their analysis is summarized as follows:

The FTIR band appearing at $\nu \sim 1,727\text{--}1,732\text{cm}^{-1}$ is assigned to the stretching vibrational mode [i.e., $\nu(\text{C=O})_s$]

of C=O group in the PMMA backbone. Addition of even a small quantity of LiClO₄ (i.e., ~8% by weight of PMMA) shifts the band toward lower side of the frequency scale, and the peak is also broadening. As the salt concentration increases further from 8% (O/Li~12) to 35% (O/Li ~2), a consistent lowering in the position of $\nu(\text{C=O})_s$ from 1,732 to 1,727 cm⁻¹ along with the systematic broadening of the peak pattern occurs when compared with that of PMMA spectrum. Such changes in the overall profile of the spectral

**Fig. 5** FTIR plot for (a) $\nu(\text{OCH}_3)_s$, (b) $\nu(\text{OCH}_3)_a$ and (c) $\nu(\text{C=O})$

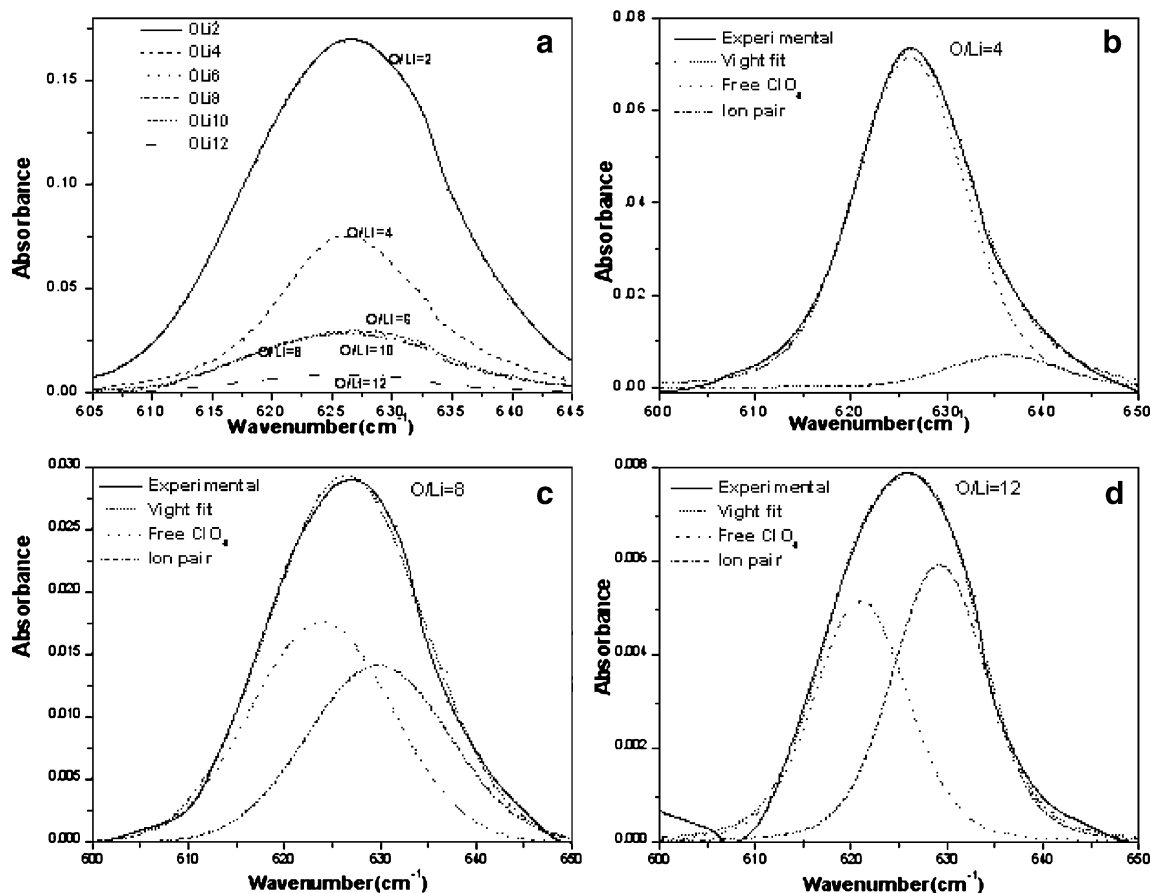


Fig. 6 FTIR plot for a (600–650 cm^{-1}) region and deconvolution of peak, b $\text{O/Li}=4$, c $\text{O/Li}=8$, d $\text{O/Li}=12$

band with increasing salt concentration provides a strong evidence of the salt interaction with polymer backbone having electron rich group, i.e., oxygen atom of the $\text{C}=\ddot{\text{O}}$ group having a lone pair of electron readily available for coordination with the electropositive atoms of the salt (i.e., Li^+ cation). For polymer films with $\text{O/Li} = 2$, the presence of bands corresponding to pure LiClO_4 (i.e., uncomplexed LiClO_4) at the wave number $\sim 1,099\text{cm}^{-1}$ has been recorded. It clearly indicates the appearance of LiClO_4 as a separate phase in PMMA- LiClO_4 bonds, suggesting that an optimum cutoff limit of salt dissolution into the polymer matrix must be at a value lower than $\text{O/Li} \sim 2$. A similar observation has already been recorded in the XRD diffractogram of the PMMA- LiClO_4 complex where a clear phase-separation for $\text{O/Li} \sim 2$ pointing toward an optimum concentration limit of the salt to be dissolved in the polymer matrix was observed.

Figure 5a–c shows the expanded pattern of FTIR spectra corresponding to $\text{C}-\text{C}-\text{O}$ stretching ($1,250\text{cm}^{-1}$) and $\nu(\text{O}-\text{CH}_3)_a$ ($1,444\text{cm}^{-1}$) and $\nu(\text{C}=\text{O})_s$ ($1,730\text{cm}^{-1}$). There is no change in band position and in intensity in $\text{C}-\text{C}-\text{O}$ stretching ($1,242\text{cm}^{-1}$) and $\nu(\text{O}-\text{CH}_3)_a$ ($1,444\text{cm}^{-1}$) region after addition of salt. As discussed above, the $\nu(\text{C}=\text{O})_s$ ($1,730\text{cm}^{-1}$) band is getting affected after the addition of

salt and it is also clear from Fig. 5c. There are two electronegative group present in PMMA ($\text{C}=\ddot{\text{O}}$ and $\ddot{\text{O}}-\text{CH}_3$), which can interact with lithium ions [15]. But these observations indicate in unambiguous terms that Li^+ ion is interacting only with $\text{C}=\ddot{\text{O}}$ group of the monomer unit in the PMMA by way of possibly a weak coordination with the active site in the polymer host matrix.

The FTIR band appearing at 844cm^{-1} is assigned to $\gamma(\text{CH})_s + \nu(\text{C}-\text{O}-\text{C})_s$. It appears from an inspection of the spectrum that no major change in the band position of this molecular combination could be observed on varying the salt (LiClO_4) concentration in the O/Li range of 12 to 4 (8–21% of PMMA in terms of weight ratio). This further indicates that there may not be any possibility of Li^+ interaction with the $\ddot{\text{O}}-\text{CH}_3$ group of the PMMA.

Finally, significant changes in the $\delta(\text{ClO}_4^-)_a$ vibrational mode of the salt appearing at the wave number $\sim 624\text{cm}^{-1}$ has been observed as the salt concentration is increased from 8% ($\text{O/Li} = 12$) to 35% ($\text{O/Li} = 2$) of PMMA (w/w). The changes of the band around $\sim 624\text{cm}^{-1}$ with addition of salt are accompanied by a marked variation of intensity (Fig. 4). In the case of ClO_4^- band occurring at 624cm^{-1} , it can easily be inferred that the band profile is asymmetric (Fig. 6a). The existence of such asymmetry arises due to

Table 3 Estimated fraction of free anion and ion-pairs in PMMA-LiClO₄ (O/Li ~0–12) films

O/Li ratio	Salt–polymer ratio (w/w)	Fraction of free anion (%)
2	35:65	42.4
4	21:79	91.1
6	15:85	45.9
8	12:88	55.3
10	10:90	66.9
12	08:92	46.4

the presence of degeneracy caused by more than one contribution. It is believed that the presence of asymmetry in the perchlorate band arises primarily due to the presence of ion pairs in addition to free ClO₄⁻ anion in the polymer matrix. To confirm this possibility, we have carried out deconvolution of the $\delta(\text{ClO}_4^-)_a$ band using a computer program “peakfit” in the spectral range 600–650cm⁻¹ for polymer films of all the salt concentration. Representative deconvoluted pattern for O/Li = 4 (21% salt), O/Li = 8 (12% salt), and O/Li = 12 (8% salt) is given in the Fig. 6b–d. It is observed from the fitted pattern that there are two distinct contributions in the spectral range 600–650cm⁻¹ appearing in the spectral ranges 620–630cm⁻¹ and 630–650cm⁻¹. They are attributed to spectroscopically “free ClO₄⁻” and presence of contact ion-pairs, respectively [16]. The fraction of free anion and contact ion pair has been calculated from the deconvoluted

spectrum profile of $\delta(\text{ClO}_4^-)$ vibrational mode using the formula:

$$\text{Fraction of free anion (FFA)} = \frac{\text{Free anion peak area}}{\text{Total peak area}} \quad (4)$$

and fraction of ion pair

$$\text{Fraction of ion pair (FIP)} = \frac{\text{Ion pair peak area}}{\text{Total peak area}} \quad (5)$$

The quantitative estimate of fraction of free anion and ion pair for all O/Li ratio is given in Table 3. It is observed that for O/Li ~4, the fraction of free anion is highest. Beyond, this salt concentration ion pairing effect appears to dominate possibly due to the formation of higher ion aggregates. Therefore, a quantification, based on FTIR results, on the fraction of free anions and ion pairs present in the sample films provide an insight into the possibility to believe that, a salt concentration ~O/Li = 4 may be the threshold limit for salt dissolution into the PMMA matrix, where highest number of free anions and hence the free cations are available for mobility from one available site to another.

Electrical analysis

The electrical properties of the solid polymer electrolyte films have been studied using the AC technique of complex impedance spectroscopy (CIS) analysis. Typical Nyquist plot of the polymer–salt complex samples for selected salt

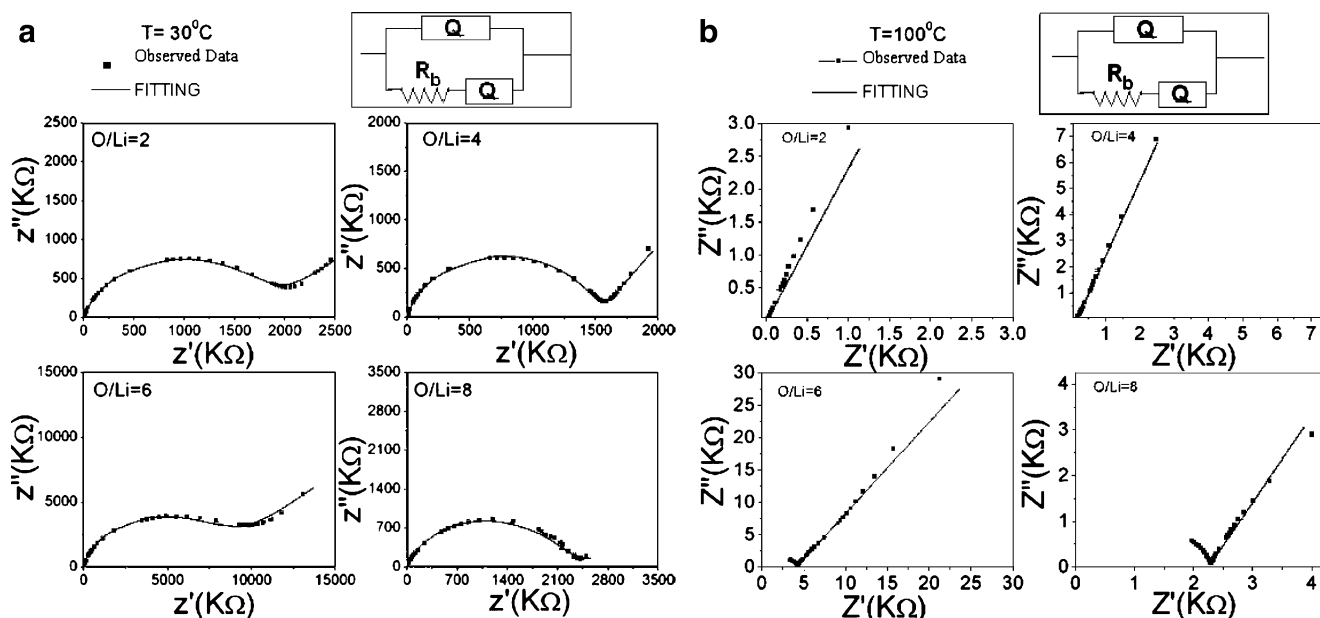
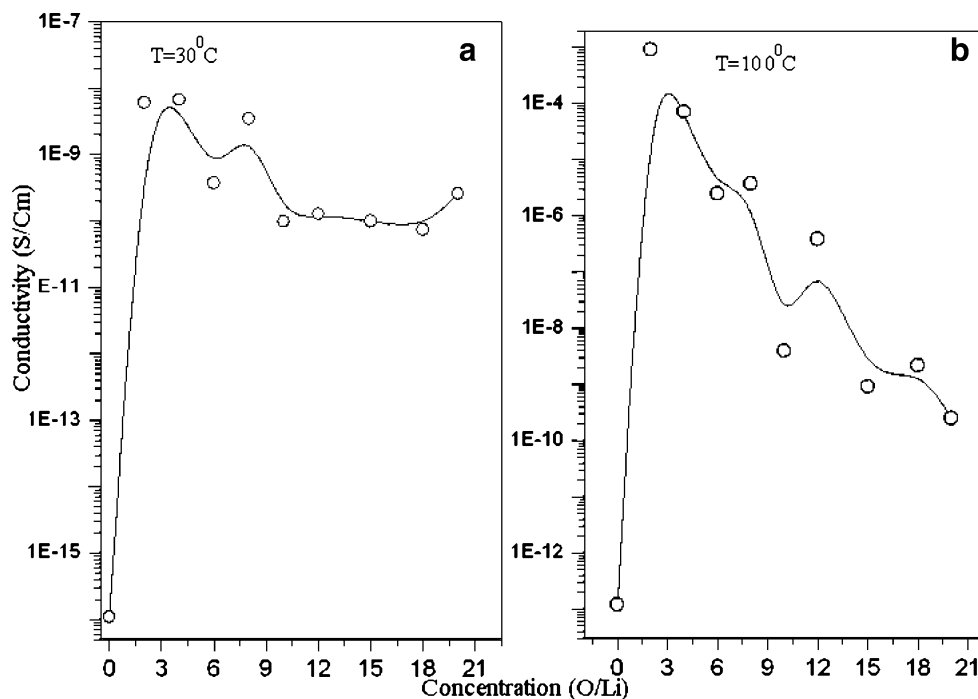


Fig. 7 **a** Impedance plot for PMMA-LiClO₄ with different O/Li ratio at $T=30$ °C; **b** impedance plot for PMMA-LiClO₄ with different O/Li ratio at 100 °C

Fig. 8 Conductivity vs. concentration (O/Li ratio) at $T=30\text{ }^{\circ}\text{C}$ and at $100\text{ }^{\circ}\text{C}$



concentration at $T \sim 30\text{ }^{\circ}\text{C}$ (Fig. 7a) and at $100\text{ }^{\circ}\text{C}$ (Fig. 7b) along with their model equivalent electrical circuit are shown in the inset of Fig. 7. The complex impedance plot at room temperature ($30\text{ }^{\circ}\text{C}$) has typical features of two well-defined regions indicated by the presence of a high-frequency semicircular arc, which is followed by another arc (that could not be completed due to lack of data) in low-frequency region. The high-frequency arc is attributed to the bulk contribution, whereas the low-frequency arc is related to the phase boundary that becomes dominant at higher salt concentration (O/Li $\sim 8\text{--}2$) due to appearance of crystalline components in the PS matrix in good agreement with the XRD results. As the temperature is increased, the pattern of evolution of the impedance spectrum changes gradually irrespective of the salt concentration. Such a change in the CIS pattern Fig. 7b driven predominantly by thermal activation has profound effect on the polymer microstructure and its electrical transport properties. The impedance spectrum now has a high-frequency arc followed by a low-frequency spike, which may be related respectively to the bulk conduction process and accumulation of charges (double-layer formation) at the electrolyte–electrode (blocking electrode) interface [17]. The corresponding electrical equivalent circuit representing the sample behavior is given in the inset for the impedance spectrum at $100\text{ }^{\circ}\text{C}$ as a representative pattern of the effect of temperature on impedance response. Furthermore, the intercept of the high frequency semicircular arc in the impedance spectrum provides us an estimate of the bulk sample resistance (DC resistance, i.e., R_b). An estimated experimental value of the bulk resistance (R_b) for each salt

concentration over a range of temperature enables us to evaluate the DC conductivity as a function of concentration and temperature.

A variation of the DC conductivity (σ_{dc}) of the PS samples as a function of temperature at 30 and $100\text{ }^{\circ}\text{C}$ is shown in Fig. 8a, b, with their absolute values recorded in the Table 1. A comparison of the conductivity results indicates that there has been a substantial enhancement in the conductivity of pure PMMA on complexation with salts, the increase being to the tune of nine orders of magnitude ($10^{-16} \rightarrow 10^{-7}\text{ S cm}^{-1}$) at $30\text{ }^{\circ}\text{C}$ and almost by the same orders

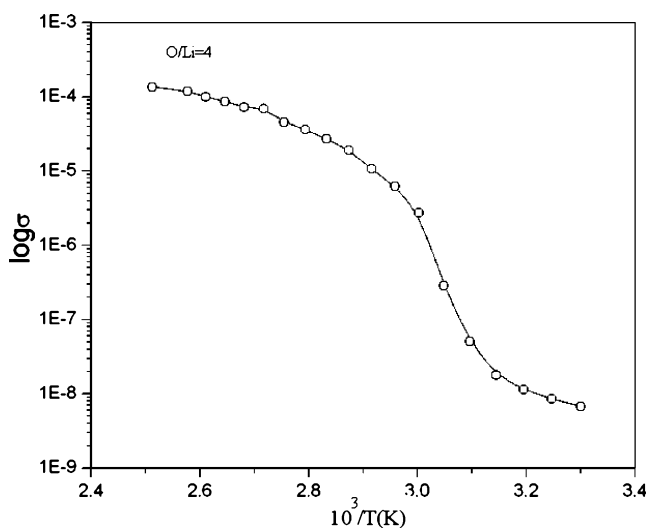


Fig. 9 Conductivity vs. temperature plot for PMMA+LiClO₄ (O/Li=4)

of magnitude (10^{-13} – 10^{-4} S cm $^{-1}$) at 100°C. The conductivity value of pure PMMA agrees well with the value reported in literature (10^{-16} S cm $^{-1}$ at room temperature) [18]. A drastic enhancement in the value of conductivity at 100°C may be directly related to the polymer chain flexibility above its glass transition ($T \geq T_g \equiv 95^\circ\text{C}$) and also due to the property of amorphous polymer electrolyte to provide a bigger free volume upon increasing the temperature, which facilitates ion migration, thereby resulting in an increase in ionic conductivity [19, 20].

Furthermore, at room temperature, an optimum value of conductivity has been observed for O/Li \sim 4. But at high temperature (100°C), the highest conductivity has been found for O/Li \sim 2. The contrasting value of electrical conductivity of the PMMA-LiClO $_4$ samples with O/Li = 2 and O/Li = 4 at room temperature ($T = 30^\circ\text{C}$) and at 100°C ($T \geq T_g$, the glass transition temperature) may be attributed to the factors such as: (1) cation coordination and salt dissolution in the solid polymer matrix to an optimum limit of salt uptake; (2) presence of undissolved salt existing as a separate phase as the ion pairs (Li $^+$ ClO $_4^-$); (3) dissociation of undissolved salt at elevated temperatures; and (4) flexibility of polymer chain above its T_g . At room temperature (30°C), the presence of undissolved salt existing as a separate phase in the form of ion pairs (Li $^+$ ClO $_4^-$) in the polymer film with O/Li = 2 is responsible for lower value of conductivity in comparison to the sample with O/Li = 4. In the latter case, salt gets fully dissolved in polymer matrix, and cations are coordinated to electron-rich site with the probability of two electron-rich sites available for each Li $^+$ cation in the polymer–salt complex matrix. In sharp contrast to this situation, at $T = 100^\circ\text{C}$ (i.e., $\geq T_g$ of the host polymer), greater dissociation of undissolved salt (LiClO $_4$) of the polymer film with O/Li = 2 may be responsible for higher value of available charge carriers for mobility through the polymer matrix. This also seems logical above T_g of the polymer host due to lowering in viscosity, reduction in internal friction and minimization of resistance to the ion migration assisted by flexible polymer chain mobility. The overall effect is an enhancement in conductivity of the polymer film sample with O/Li = 2 unlike in the sample with O/Li = 4 at 100°C.

A variation of DC conductivity (σ_{dc}) as a function of temperature for the optimized PMMA-LiClO $_4$ (O/Li \sim 4) is shown in the Fig. 9. It shows a typical Vogel–Tamman–Fulcher (VTF) type conduction behavior governed by the relation:

$$\sigma = \sigma_0 \exp \frac{[-E_a]}{k_\beta(T - T_0)} \quad (6)$$

where σ_0 ($=AT^{-1/2}$) is the pre-exponential factor, A is a constant that depends upon the number of carrier ions, $k_\beta =$

Boltzmann constant, E_a is the activation energy, and T_0 is a fitting parameter called reference temperature and identified as the glass transition temperature (T_g) of the polymer host below which the polymer chain motion of the polymer matrix is completely stopped [21]. According to the VTF model, ionic conduction at high temperature occurs as a result of cooperative segmental motion of polymer matrix. Above T_m , the polymer matrix undergoes a phase transition and behaves as a viscous liquid, in spite of having a solid nature in terms of its physical dimensions, and offers less internal friction for mobile ions, thereby facilitating ion transport at a faster rate resulting in an enhancement in conductivity.

Conclusions

The present work reports experimental studies on the optimization of salt concentration in a PMMA-based solid polymer electrolyte system with reference to electrical conductivity, structural phase stability, and the optimum threshold limit of salt dissolution in the polymer host matrix. Experimental analysis carried out on a PS film prepared using the standard solution-cast technique over a range of salt concentration reveals that: (1) phase-separation in the polymer salt complex occurs at O/Li \geq 2 (35% salt w. r.t. PMMA w/w); (2) an optimized conductivity has been observed for O/Li \sim 4 (21% salt w.r.t. PMMA w/w); (3) unambiguous evidence of cation coordination at the C=O site in the polymer backbone out of the two possible sites, i. e., C=O and (O–CH $_3$), i.e., polymer–salt interaction; (4) evidence of ion–ion interaction, which is strongly the function of salt concentration, has been observed; (5) salt concentration dependent ion–ion interaction may be the primary factor controlling the concentration dependence of conductivity; and (6) electrical conductivity obeys VTF behavior, suggesting liquid type ion transport in a solid polymer electrolyte matrix at a temperature above its T_m .

Acknowledgment Authors acknowledge with thanks the financial support received from the Ministry of Human Resource Development (MHRD), Govt. of India, New Delhi for the financial support received vide grant no.: MHRD/RD/F.IV, dated 31st March 2005 for carrying out this piece of research at the Department of Physics & Meteorology, IIT, Kharagpur 721302, INDIA.

References

1. Ries ME, Breton MG, Cruickshank JM, Klein PG, Ward I (1995) *Macromolecules* 28:3282–3289
2. Hussain R, Mohammad D (2004) *Turk J Chem* 28:725–729
3. Chen HW, Lin TP, Chang FC (2002) *Polymer* 43:5281–5288
4. Appetecchi GB, Croce F, Scrosati B (1995) *Electrochimica Acta* 40:991–997

5. Bohnke O, Frand G, Rezzazi M, Rousselot C, Truche C (1993) *Solid State Ionics* 66:97–104
6. Wieczorek W, Stevens JR (1997) *J Phys Chem B* 101:1529–1534
7. Ali AMM, Yahya MZA, Bahron H, Subban RHY, Harun MK, Atan I (2007) *Mater Lett* 61:2026–2029
8. Kumar R, Sharma JP, Sekhon SS (2005) *Eur Polym J* 41:2718–2725
9. Rajendran S, Uma T (2000) *Bull Mater Sci* 23:27–29
10. Uma T, Mahalingam T, Stimming U (2005) *Mater Chem Phys* 90:245–249
11. Ren T, Huang X, Zhao X, Tang X (2003) *Mater Sci* 38:3007–3011
12. Stuart BH (2004) *Infrared spectroscopy: fundamentals & applications*. Wiley, New York
13. Hummel DO (1966) *Infrared spectra of polymers in the medium and long wavelength regions*. Wiley, New York
14. Licoccia S, Trombetta M, Capitani D, Proietti N, Romagnoli P, Vona LD (2005) *Polymer* 46:4670–4675
15. Song JY, Wang YY, Wan CC (1999) *J Power Sources* 77:183–97
16. Wieczorek W, Zalewska A, Raducha D, Florjanczyk Z, Stevens JR (1996) *Macromolecules* 29:143–155
17. Kim C, Lee G, Lio K, Rhu KS, Kang OSG, Chang SH (1999) *Solid State Ionics* 123:251–257
18. Adamec V, Mateova E (1975) *Polymer* 16:166–168
19. Druger SD, Ratner MA, Nitzam A (1985) *Phys Rev B* 31:3939–3947
20. Miyamoto T, Shibayama K (1973) *J Appl Phys* 44:5372–5376
21. Tamman VG, Hesse HZ (1926) *Anorg Allg Chem* 19:245